THE JOURNAL OF PHYSICAL CHEMISTRY C
A JOURNAL OF THE AMERICAN CHEMICAL SOCIETY

pubs.acs.org/JPCC

Article

In Situ Reactive TEM Study of the Oxidation Kinetics of Aluminum Nanoparticles

Keren Shi and Michael R. Zachariah*

Cite This: https://doi.org/10.1021/acs.jpcc.5c06533

Read Online

ACCESS | Metrics & More | Article Recommendations | Supporting Information

ABSTRACT: This study evaluates the oxidation kinetics of aluminum nanoparticles from 25 to 1000 °C by *in situ* reactive cell transmission electron microscopy. Combined with TGA-DSC measurement, the oxidation can be divided into three stages from 25 to 1000 °C. The first heating stage is absent any discernible chemistry from 25 to ∼600 °C. A low temperature oxidation stage from ∼600 to ∼800 °C, with an irregular volume increase, where the reaction rate is limited by oxygen diffusing through the alumina shell. A third high-temperature oxidation stage from ∼800 to 1000 °C, corresponding to Al diffusing outward through the alumina shell, ultimately leads to hollow particles. Using quantitative temporal imaging of the evolution of the particle morphology under oxidation conditions, a reaction flux and diffusivity are determined. Comparison with other methods in the literature, we find a clear trend that the measured diffusivity scales with heating rate, which likely explains the wide disparity of diffusivities reported in the literature.

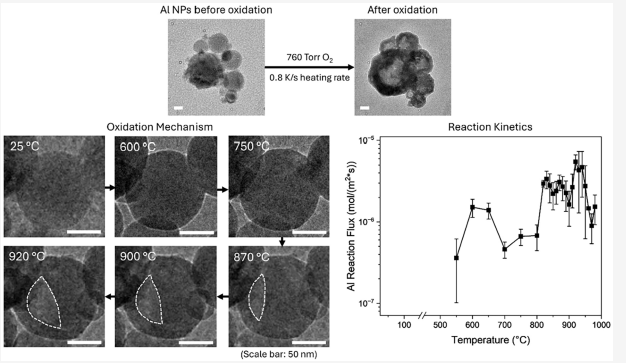

1. INTRODUCTION

Aluminum (Al) nanoparticles have high reactivity and energy density,[1−3] and are widely used in thermites, propellants, and explosives to improve combustion performance.[4−6] As such, an understanding of the mechanisms and kinetics of oxidation is of great relevance. While there are numerous studies on aluminum combustion in various formulations, studies of the microscopic properties of oxidation are more limited. Firmansyah et al. studied Al nanoparticle oxidation by in situ X-ray diffraction and discovered that the alumina shell fractured at or near the melting point of Al, with the local phase transformation of amorphous alumina to γ phase allowing Al to expand.[7] Trunov et al. investigated alumina shell phase transformations, which they were able to relate to the mass increase stages observed in thermal analysis.[8] They were able to show how the initial amorphous native alumina shell transitioned to γ phase and then to α-alumina during oxidation. Zhang et al. examined different models and concluded that the best fit to thermogravimetric experiments implied the reaction takes place at the outer surface of the shell.[9] Henz et al. used molecular dynamics simulation to investigate the diffusion mechanism with various particle diameters and alumina shell crystallinity.[10] They found that strong electric fields induced with the oxide shell contributed to a rapid Al-ion flux. These studies suggest that direct visualization of oxidation would be very helpful in both the mechanistic and quantitative evaluation of controlling processes.

With the rapid development of in situ transmission electron microscopy (TEM) technology, we now have an opportunity to observe in real-time the morphological changes under environmental conditions (e.g., gas environment, electrochemical stimulation, or ultrafast heating).[11−13] However, only a few studies have been reported regarding the oxidation of Al nanoparticles. The oxidation of Al nanoparticles has been studied by Gao et al.[14] They focused on alumina shell growth during oxidation. They observed partial amorphous-to-crystalline transformation and nanocrack formation on the shell at low temperature and formation of γ-Al_2O_3 at high temperature. Zhou et al. studied Al nanoparticles oxidation and concluded that the oxidation and shell breakage were related to particle size.[15] The formation of protrusions was caused by the buildup of internal stress and crystal alumina formation. In-situ TEM provided a direct characterization of the phase transformation of the alumina shell and the morphology change of the nanoparticle. However, there has been no report of extracting reaction kinetics, which we will be exploring in this work.

Received: September 18, 2025
Revised: December 21, 2025
Accepted: December 22, 2025

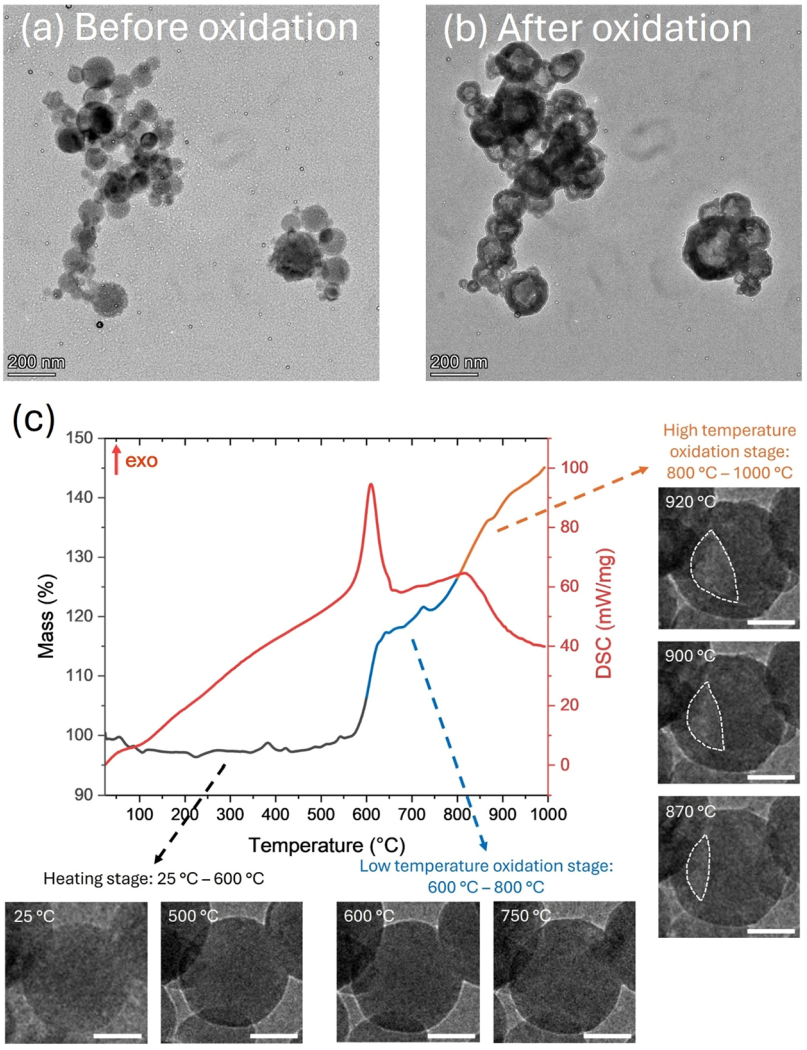

Figure 1. (a) TEM image of Al nanoparticles at 25 °C before oxidation. (b) TEM image of Al nanoparticles after oxidation in ∼760 Torr oxygen to 1000 °C at 0.8 K/s heating rate. (c) TGA-DSC of Al nanoparticles under oxidation in oxygen at 0.8 K/s heating rate and morphology change of the same Al nanoparticle at different oxidation stages from in situ TEM. The complete image sequences are shown in Figure S2. (scale bar: 50 nm).

In this study, we applied in situ reactive TEM to directly visualize the morphology evolution of ∼100 nm Al nanoparticles in a ∼760 Torr oxygen environment during heating from 25 to 1000 °C. The oxidation process was identified in conjunction with TGA-DSC measurements. Quantitative analysis of the temporal TEM images enabled the extraction of reaction fluxes and effective Al diffusivities, demonstrating an approach for deriving kinetic parameters directly from in situ TEM measurements. This integrated method establishes a framework for probing oxidation kinetics at the particle level and the mechanism study of reactive metal nanoparticles.

2. EXPERIMENTAL METHODS

2.1. Material and Sample Preparation

Aluminum nanoparticles (Al, 100 nm) were purchased from US Research Materials. The active content was 75 wt % measured by thermogravimetric analysis. To prepare the nanoparticles for transmission electron microscopy (TEM) experiments, ∼1 mg of Al nanoparticles was mixed with 2 mL of hexane (Honeywell). The solution was sonicated for 15 min and drop-cast on the in situ TEM chips (Protochips) with silicon nitride windows.

2.2. In Situ TEM Characterization

TEM images and videos were taken with a Titan Themis 300 (ThermoFisher Scientific) operated at 300 kV in bright-field TEM mode by using an FEI Ceta camera with an acquisition time of 125 ms per frame. The images were collected under slight defocus (−3 to −5 μm), and focus was continuously optimized during in situ heating. A 100 μm objective aperture was used to enhance the image contrast. The gas environment and temperature of the in situ TEM holder were controlled by Protochips ATMOSPHERE AX. Prior to the experiment, the in situ holder was pumped down to ∼1 Torr and refilled with ∼760 Torr Oxygen for 5 cycles to remove the residual gas from the system. For the in situ heating experiment, the holder environment was set at ∼760 Torr Oxygen with a flow rate of 1 sccm. The temperature was set to heat from 25 to 1000 °C with a heating rate of 0.8 °C/s. To minimize electron beam irradiation on the Al nanoparticles, images were taken from 25 to 600 °C at 50 °C intervals. The morphology changes of particles from 600 to 1000 °C were recorded by videos at ∼7 fps. The in situ experiment was repeated twice under the same environmental and heating conditions. The beam currents for the two runs were 8.78 and 7.76 nA, corresponding to electron

https://doi.org/10.1021/acs.jpcc.5c06533
J. Phys. Chem. C XXXX, XXX, XXX−XXX

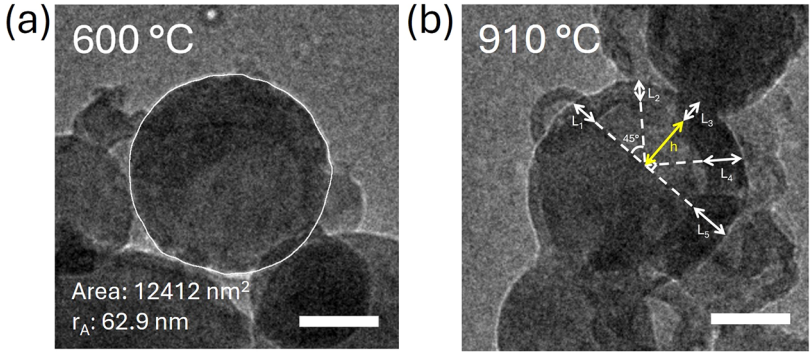

Figure 2. (a) Volume calculation from the projected area (area inside the white line) of the Al sphere. The shape-induced uncertainty is discussed in Supporting Information Discussion 3. (b) Height of the hollow spherical cavity and shell thickness measurement used to calculate the volume of the hollow region. The shell thickness (L) is averaged from 5 different measurements. (Scale bar: 50 nm).

dose rates of 2.15×10^3 and 2.77×10^3 $e^-/nm^2/s$, respectively. Nine individual Al nanoparticles, whose diameters were ~100 nm, were further analyzed to obtain reaction flux and diffusivity.

2.3. Thermogravimetric Analysis (TGA)

The mass change and heat release from oxidation of Al nanoparticles were characterized by thermogravimetric Analysis (TGA) with differential scanning calorimetry (DSC, STA 449 F3 Jupiter, NETZSCH). The Al nanoparticles were heated from room temperature to 1000 °C at 0.8 °C/s (same as in situ TEM experiments) and 0.167 °C/s with an oxygen flow of 50 mL/min.

3. RESULTS AND DISCUSSION

3.1. Correlating Thermal Analysis with *In Situ* TEM

The Al particles employed for this study were obtained from US Research Nanomaterials and are shown in Figure 1a. The particles show a wide size distribution ranging from ~20 to ~200 nm, with an average primary size of ~100 nm. Figure 1b shows Al nanoparticles postoxidation in ~760 Torr oxygen at 1000 °C, at a heating rate of 0.8 K/s, and clearly shows that after oxidation, the primary particles are hollow with a thick oxide shell. The fact that particles with different diameters show the same resulting morphology implies the oxidation mechanism is not related to size. Previous studies have suggested that the TEM electron beam can induce changes in metal nanoparticles.[11,16] To minimize the beam effect on the samples, Al nanoparticles were first evaluated in a TGA to identify the reaction temperature region from 25 to 1000 °C at 0.8 K/s in an oxygen flow (Figure 1c). Since Al nanoparticles are reactive, ~0.5 mg samples were used to avoid unintended ignition inside the instrument. The resulting mass changes were noisy, but the mass gain trend matched the experiment performed with a 0.167 K/s heating rate, and it was used to identify the oxidation stages. The mass increase initiates at ~600 °C, before the melting point of Al, and is consistent with prior observations by others.[17,18] Based on the TGA results, TEM images were taken from 25 to 600 °C at every 50 °C increment, and videos were recorded from 600 to 1000 °C to study the oxidation process. The Al nanoparticles that were not irradiated by the electron beam (Figure S1) were compared with the nanoparticles that were under continuous imaging, and showed the same hollow structures with thick shells after oxidation. Thus, we may assume that the electron beam had a minimal influence on the oxidation process.

The reactive TEM images of the same Al nanoparticle in Figure 1c show the morphological changes in different oxidation stages. Based on the mass increase measured by TGA and morphology changes imaged by in situ TEM, the oxidation process of Al nanoparticles can be divided into three stages from 25 to 1000 °C. The first stage from 25 to ~600 °C, shows no significant mass increase (TGA), and no thermal events (DSC). The projected areas from the TEM images show an increase in size. These volume increases were calculated using the area-equivalent radius (r_A) from the projected area in TEM images at 25 and 550 °C (r_A was measured by the method shown in Figure 2a). The measured average volume increase was 1.4 ± 0.5% (SD), which is less than the expected theoretical volume increase of 4.2% calculated from the molar volume of Al at 25 and 550 °C[19] (Figure S3). These results imply that the alumina shell is rigidly confining the Al core, and thus, there must also be a pressure increase inside the alumina shell from Al lattice thermal expansion. The calculated pressure increase in the Al core is ~0.7 GPa, assuming the Al thermal expansion is isotropic.[7] This estimated pressure is ~3× higher than values (~0.2 GPa) obtained from X-ray diffraction measurements of lattice spacing.[7,20,21] Since our approach relies on an area-equivalent radius rather than direct lattice spacing imaging, this discrepancy indicates that this method is not accurate for determining lattice scale pressures. The second stage observed is the low-temperature oxidation from ~600 to ~800 °C. The TGA-DSC results show a mass increase corresponding with an exotherm which occurs prior to the melting of Al. The melting point is ~655 °C, determined by the peak of the endotherm. In this regime, the external surface of the particles becomes irregular and the projected area increases. There are no significant contrast changes to the Al core region in the TEM images. Although in this experiment the reaction mechanism at low temperature oxidation stages cannot be directly observed, prior work of others, suggests that oxidation takes place by oxygen diffuse through the alumina shell in the low temperature oxidation stage.[14,22] However, other models propose that oxidation may occur at the outer surface of the alumina shell, governed by outward Al diffusion.[9,10] The third stage is the high temperature oxidation from ~800 to 1000 °C, corresponding to a continuous mass increase and another exothermic peak in the DSC. The in situ TEM images show a brighter region with a well-defined internal interface form in the Al core, which keeps increasing with temperature, indicating the Al core begins to hollow out (outlined with a

https://doi.org/10.1021/acs.jpcc.5c06533
J. Phys. Chem. C XXXX, XXX, XXX−XXX

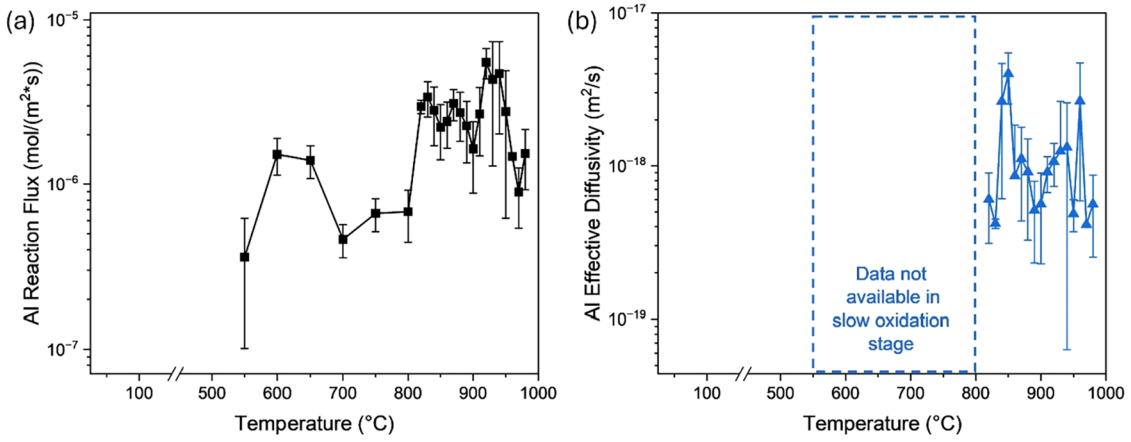

Figure 3. (a) Averaged Al reaction flux measured from in situ TEM during oxidation from nine individual nanoparticles (error bar represents the standard deviation of the measurements). (b) Effective Al outward diffusivity in the high-temperature oxidation stage.

dashed line in Figure 1c). The shell thickness continually increases during this process, associated with the external formation of alumina. A video of the complete oxidation process is shown in video S1.

3.2. Extracting Kinetic Parameters

We next turned our attention to extracting kinetic parameters from the temporal images. In the low temperature oxidation stage, the average volume increase is 17.8 ± 2.2% (SD) measured from TEM images (Figure S4). The theoretical volume increase of γ and α-alumina is only ~3% from linear thermal expansion.[8,23,24] So we assume that the volume increase was from alumina formation and the reaction flux ($J_{\text{low-temp}}$) can be calculated by eq 1:

$$J_{\text{low-temp}} = \frac{\frac{d\ \text{mol}_{\text{Al}}}{dt}}{A_{\text{outer surface}}} \tag{1}$$

where $A_{\text{outer surface}}$ is the area of the outer surface of the nanoparticle, mol_{Al} is the moles of reacted Al calculated from the particle volume increase, and t is the heating time of the experiment (detailed equation shown in Supporting Information Discussion 1).

For the reaction flux at the high-temperature oxidation stage, the contrast within the core denotes regions where the particle has emptied out (lighter regions) inside Al nanoparticles. This region is assumed to be empty and forms a hollow spherical cavity inside the alumina shell. From the imaging, the volume of the empty region (V_{cap}) is calculated by eq 2:

$$V_{\text{cap}} = \frac{\pi h^2}{3}(3r_{\text{core}} - h) \tag{2}$$

where h is the height of the cavity. The radius of the Al core inside the alumina shell (r_{core}) is calculated by $r_{\text{core}}=r_{\text{A}}-L$ (L is the average shell thickness shown in Figure 2b). The flux at the high-temperature stage ($J_{\text{high-temp}}$) can be expressed by eq 3:

$$J_{\text{high-temp}} = \frac{\frac{d\ \text{mol}_{\text{liquid Al}}}{dt}}{A_{\text{outer surface}}} \tag{3}$$

where $\text{mol}_{\text{liquid Al}}$ is the moles of liquid Al inside the oxidation shell (Supporting Information, Discussion 2).

The calculated Al reaction flux is plotted in Figure 3a and shows bimodality as a function of temperature. It first shows a peak from ~600 to ~650 °C corresponding to the first mass increase region seen in the TGA (Figure 1c), and the second peak from ~800 to ~900 °C corresponds to the second mass increase region shown in the TGA. The oxygen flux (J_{O_2}) to a particle can be expressed by eq 4:

$$J_{\text{O}_2} = \frac{1}{4}n\bar{\nu} = \frac{1}{4}\frac{P}{RT}\bar{\nu} \tag{4}$$

where P is the oxygen pressure inside the in situ TEM holder, T is the temperature of the in situ TEM holder, $\bar{\nu}$ is the mean molecular speed of oxygen, and R is the gas constant. Evaluation of eqs 2−4 shows that oxygen flux is ~10^9 times larger than the reaction flux (Figure S5), and suggests that in the low temperature oxidation stage, the reaction rate is limited by the oxygen diffusion through the alumina shell. While in the high-temperature oxidation stage, TEM images showed hollow core formation, indicating outward Al diffusion. However, whether oxidation is limited by only Al diffusion to the shell exterior or by coupled Al and oxygen diffusion within the shell cannot be resolved in this experiment.

From the reaction flux, we can extract an effective Al diffusivity with some approximations. Due to the magnification used in the in situ TEM experiment, the alumina shell thicknesses during the low temperature oxidation stage cannot be determined based on poor image contrast. So the effective diffusivity was only calculated at the high temperature oxidation stage under the assumption that oxidation is the Al transport limit by Fick's law (eq 5),

$$D_{\text{high-temp}} = -\frac{J_{\text{high-temp}}}{\frac{dc_{\text{liquid Al}}}{dL}} \tag{5}$$

where $c_{\text{liquid Al}}$ is the concentration of liquid Al inside the oxide shell of the nanoparticle (Supporting Information Discussion 4). The results are plotted in Figure 3b and show no clear temperature dependence, likely due to the relatively large standard deviation between measurements. The average diffusivity is determined to be ~1.2×10^{-18} m^2/s in the high temperature oxidation stage.

It is well-known that for small oxide layer thicknesses, field-assisted ion mobility can be the major driving force for transport through the oxide layer, and has been described by the Carrera-Mott (CM) theory.[25] The basic premise is that differences in the chemical potential of the electron at the interface result in charge injection from the more-electro-

https://doi.org/10.1021/acs.jpcc.5c06533
J. Phys. Chem. C XXXX, XXX, XXX−XXX

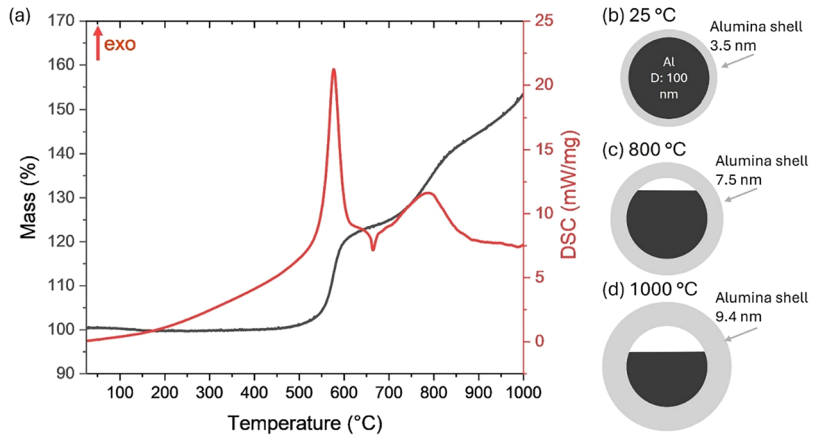

Figure 4. (a) TGA-DSC results of Al nanoparticles oxidation at 10 °C/min. (b) The scheme of a 75 wt % Al nanoparticle with a 100 nm Al core has approximately 3.5 nm alumina shell. Scheme of an Al nanoparticle oxidation at (c) 800 °C and (d) 1000 °C. Alumina shell thicknesses were calculated by the mass increase from TGA. (Note: the schemes were not drawn to scale).

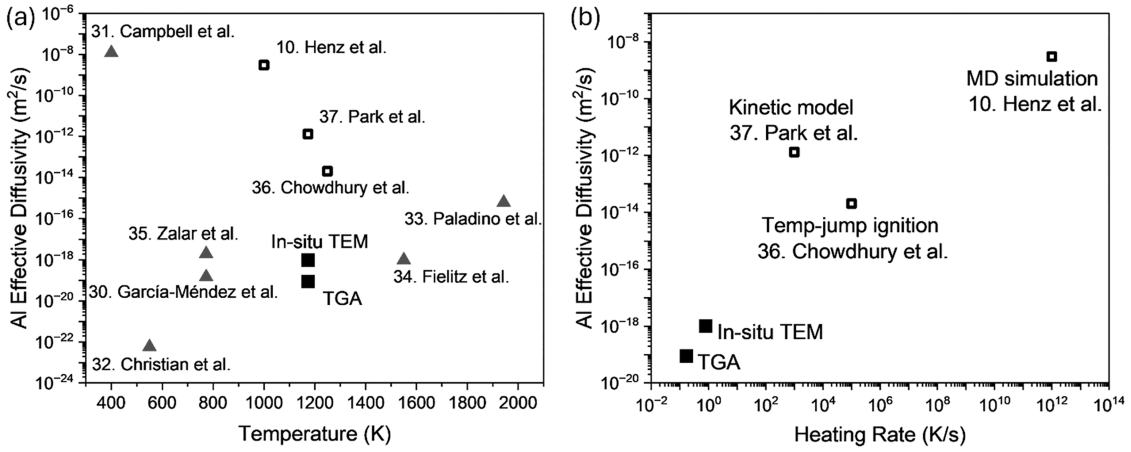

Figure 5. (a) Al diffusivity in alumina as a function of temperature from literature and determined in this study. (b) Comparison of Al diffusivities obtained at different heating rates from this study and previous works from our group. (■ represent results from this study, □ represents previous results from our group, ▲represents literature data).

positive region. In this case from the Al to Al_2O_3, resulting in a steady-state electric field, which can be quite large (>10^8 V/m) for oxide thicknesses of a few nm's.[10] When the aluminum core melts, Al ions are driven through the oxide shell governed by the Nernst–Planck equation, assuming an intact oxide layer (i.e., no metallic percolation/shorting). As Al ions begin to migrate through the layer, the field will begin to collapse unless counteranions arrive to sustain the field. The characteristic charge-relaxation or Maxwell time (τ) is given by eq 6:[26]

$$\tau = \frac{\varepsilon}{\sigma} \tag{6}$$

where $\varepsilon = \varepsilon_r\varepsilon_0$ is the permittivity of the oxide, ε_0 is the vacuum permittivity, and ε_r is the relative permittivity. σ is the ion conductivity. If τ is much less than the oxidation time scale, the field collapses.

Let us now estimate if, given our conditions, field-assisted transport is important. Using our measured values of $D_{high-temp}$ (1.2×10^{-18} m^2/s), $J_{high-temp}$ (2.8×10^{-6} mol/(m^2×s)), and the average shell thickness (L = 21 nm) at 1000 °C, we can estimate the steady-state Al ion concentration (n) in the oxide layer by eq 7:

$$n \approx \frac{J_{high-temp} \times N_A \times L}{D_{high-temp}} \approx 2 \times 10^{28}\, m^{-3} \tag{7}$$

The Nernst–Einstein ion-conductivity (σ) is then approximated as eq 8:[27]

$$\sigma \approx \frac{z^2 e^2 n D_{high-temp}}{k_B T} \approx 5 \times 10^{-7}\ \mathrm{S/m} \tag{8}$$

where z is the charge number of the Al ion, e is the elementary charge, and k_B is the Boltzmann constant. From eq 6, using ε_r = 9 for alumina,[28] we obtain a charge-relaxation time of ~0.16 ms. This implies that if the oxidation time is larger than the relaxation time, which in our case, it certainly is, the built-in electric field will collapse, and in the absence of any substantial defects, the effective diffusion coefficient measured in our experiment is Fickian in nature and justifies its derivation from the measured flux.

As an alternative approach, we evaluated the effective diffusivity from the extent of reaction from the TGA measurement. The TGA measurements were performed at a 0.167 °C/s heating rate to obtain more accurate results (Figure 4a), but still close to the 0.8 K/s used in the TEM experiments. The TG and DSC curves shift to a lower temperature due to

https://doi.org/10.1021/acs.jpcc.5c06533
J. Phys. Chem. C XXXX, XXX, XXX−XXX

the lower heating rate. However, the overall oxidation behavior and stages remain consistent between the two heating rates. In order to make this evaluation, we assume dense α-Al_2O_3 and that the Al-oxide interfacial geometry remains unchanged during oxidation. For a particle with a 100 nm Al core before oxidation, the alumina shell thickness is calculated to be 3.5 nm based on the measured active content (Figure 4b), and this result agrees well with the average shell thickness of 3.2 nm from TEM images (Figure S6).

The mass increase is 36% at 800 °C. By assuming the Al diffuses out of the alumina shell and reacts with oxygen, the shell thickness should increase to 7.5 nm, and the concentration of the Al inside would be 7.5×10^4 mol/m^3 (Figure 4c). At 1000 °C, the alumina shell thickness should increase to 9.4 nm, and the concentration of Al in the core decreases to 6.2×10^4 mol/m^3 (Figure 4d). Using the above values, the calculated diffusivity by eq 5, yields $\sim 9 \times 10^{-20}$ m^2/s from 800 to 1000 °C. In contrast, the measured shell thickness measured from TEM images were ~17 and ~22 nm at 800 and 1000 °C, which is ~2× larger compared to the calculation. This suggests that newly formed alumina has a low density, presumably due to the defect formation during the oxidation, which is consistent with observations from other studies.[7,14,15]

Unfortunately, the literature for Al effective diffusivity in alumina is relatively sparse across temperature and reported values exhibit extremely large variability, ranging from many orders of magnitude from 10^{-22} to 10^{-8} m^2/s[29−34] (Figure 5a). In our own group, we have determined effective diffusivities from various experimental and simulation approaches.[10,35,36] In Figure 5b, we present results as a function of heating rate and clearly show a trend that higher heating rates lead to higher apparent diffusivities. This may be one reason for the very large disparity of diffusivities reported. It may be that diffusivities are dependent on the thermal driving force applied, and that a choice of diffusion coefficient should be, when possible, in a regime of heating rates close to the application. The fundamental reasons for this behavior are beyond the scope of this study, but they do point to the need for further study.

4. CONCLUSIONS

This study investigated the oxidation process of Al nanoparticles by in situ reactive TEM. Combined with TGA-DSC measurement, the oxidation can be divided into three stages from 25 to 1000 °C. The first heating stage is absent any discernible chemistry from 25 to ~600 °C. A low temperature oxidation stage from ~600 to ~800 °C, with an irregular volume increase, where the reaction rate is limited by oxygen diffusing through the alumina shell. A third high-temperature oxidation stage from ~800 to 1000 °C corresponds to Al diffusing outward through the alumina shell to ultimately lead to hollow particles. Using temporal imaging of the evolution of the particle morphology in the reactive TEM spectroscopy, a reaction flux and diffusivity are determined. Comparison with other methods in the literature, we find a clear trend that the measured diffusivity scales with heating rate, which likely explains the wide disparity of diffusivities reported in the literature.

■ ASSOCIATED CONTENT

Supporting Information

The Supporting Information is available free of charge at https://pubs.acs.org/doi/10.1021/acs.jpcc.5c06533.

In situ TEM image sequences and videos; particle circularity and volume uncertainty analysis; oxide shell thickness measurements; supporting information kinetic and effective diffusivity analysis (PDF)

Video 1 (MP4)

■ AUTHOR INFORMATION

Corresponding Author

Michael R. Zachariah − *University of California, Riverside, California 92521, United States;* orcid.org/0000-0002-4115-3324; Email: mrz@engr.ucr.edu

Author

Keren Shi − *University of California, Riverside, California 92521, United States*

Complete contact information is available at: https://pubs.acs.org/10.1021/acs.jpcc.5c06533

Notes

The authors declare no competing financial interest.

■ ACKNOWLEDGMENTS

The authors thank the support of AFOSR and MSEE DTRA University Research Alliance.

■ REFERENCES

(1) Zha, M.; Lv, X.; Ma, Z.; Zhang, L.; Zhao, F.; Xu, S.; Xu, H. Effect of Particle Size on Reactivity and Combustion Characteristics of Aluminum Nanoparticles. *Combust. Sci. Technol.* **2015**, *187* (7), 1036−1043.

(2) Sun, J.; Pantoya, M. L.; Simon, S. L. Dependence of Size and Size Distribution on Reactivity of Aluminum Nanoparticles in Reactions with Oxygen and MoO3. *Thermochim. Acta* **2006**, *444* (2), 117−127.

(3) Flannery, M.; Desai, T. G.; Matsoukas, T.; Lotfizadeh, S.; Oehlschlaeger, M. A. Passivation and Stabilization of Aluminum Nanoparticles for Energetic Materials. *J. Nanomater.* **2015**, *2015* (1), No. 682153.

(4) Ahn, J. Y.; Kim, S. H. Encapsulation of Aluminum Nanoparticles within Copper Oxide Matrix for Enhancing Their Reactive Properties. *Chem. Eng. J.* **2017**, *325*, 249−256.

(5) Liao, X.; Pei, J.; Xie, P.; Hu, Y.; Liu, J. Aluminum Particle Agglomeration Characteristics and Suppression Method during the Combustion of Aluminum-based Solid Propellants: A Review. *Propellants Explo Pyrotec* **2024**, *49* (1), No. e202300131.

(6) Lewis, W. K.; Rumchik, C. G.; Smith, M. J.; Fernando, K. A. S.; Crouse, C. A.; Spowart, J. E.; Guliants, E. A.; Bunker, C. E. Comparison of Post-Detonation Combustion in Explosives Incorporating Aluminum Nanoparticles: Influence of the Passivation Layer. *J. Appl. Phys.* **2013**, *113* (4), No. 044907.

(7) Firmansyah, D. A.; Sullivan, K.; Lee, K.-S.; Kim, Y. H.; Zahaf, R.; Zachariah, M. R.; Lee, D. Microstructural Behavior of the Alumina Shell and Aluminum Core Before and After Melting of Aluminum Nanoparticles. *J. Phys. Chem. C* **2012**, *116* (1), 404−411.

(8) Trunov, M. A.; Schoenitz, M.; Dreizin, E. L. Effect of Polymorphic Phase Transformations in Alumina Layer on Ignition of Aluminium Particles. *Combust. Theory Modell.* **2006**, *10* (4), 603−623.

(9) Zhang, S.; Dreizin, E. L. Reaction Interface for Heterogeneous Oxidation of Aluminum Powders. *J. Phys. Chem. C* **2013**, *117* (27), 14025−14031.
(10) Henz, B. J.; Hawa, T.; Zachariah, M. R. On the Role of Built-in Electric Fields on the Ignition of Oxide Coated Nanoaluminum: Ion Mobility versus Fickian Diffusion. *J. Appl. Phys.* **2010**, *107* (2), No. 024901.
(11) Rezkallah, J.; Moldovan, S.; Sauvage, X. In Situ and Operando TEM Study of Pt-Based Hollow Nanocatalysts: Tracking Morphological Changes and Reaction Products during CO2 Hydrogenation. *Appl. Catal., B* **2025**, *378*, No. 125637.
(12) Dachraoui, W.; Kühnel, R.-S.; Kummer, N.; Battaglia, C.; Erni, R. Enhanced Solid Electrolyte Interphase Layer in Li-Ion Batteries with Fluoroethylene Carbonate Additives Evidenced by Liquid-Phase Transmission Electron Microscopy. *ACS Nano* **2025**, *19* (20), 19213−19224.
(13) Zhu, X.; Wang, Q.; Shan, L.; Jung, B. O.; Choi, M.; Song, S.; Namkung, S.; Kang, N.; Shin, H.-Y.; Joo, M.; et al. Direct Observation of the Interface Reaction Dynamics of the NdCeFeB Phase via in Situ Annealing & Quenching STEM. *RSC Adv.* **2025**, *15* (1), 593−601.
(14) Gao, J.; Yan, J.; Zhao, B.; Zhang, Z.; Yu, Q. In Situ Observation of Temperature-Dependent Atomistic and Mesoscale Oxidation Mechanisms of Aluminum Nanoparticles. *Nano Res.* **2020**, *13* (1), 183−187.
(15) Zhou, Z.; Liu, Q.; Bai, Z.; Chai, L.; Zhang, N.; Jiang, H.; Deng, Z.; Zhao, W. In Situ TEM Heating Study on the Oxidation and Shell-Breaking Characteristics of Aluminum Nanoparticles with Different Diameters. *J. Phys. Chem. C* **2025**, *129* (19), 8985−8995.
(16) Jiang, N. Electron Beam Damage in Oxides: A Review. *Rep. Prog. Phys.* **2016**, *79* (1), No. 016501.
(17) Saceleanu, F.; Atashin, S.; Wen, J. Z. Investigation of the Effects of Phase Transformations in Micro and Nano Aluminum Powders on Kinetics of Oxidation Using Thermogravimetric Analysis. *Phys. Chem. Chem. Phys.* **2017**, *19* (29), 18996−19009.
(18) Eisenreich, N.; Fietzek, H.; del Mar Juez-Lorenzo, M.; Kolarik, V.; Koleczko, A.; Weiser, V. On the Mechanism of Low Temperature Oxidation for Aluminum Particles down to the Nano-Scale. *Propellants, Explos., Pyrotech.* **2004**, *29* (3), 137−145.
(19) Kozyrev, N. V.; Gordeev, V. V. Thermodynamic Properties and Equation of State for Solid and Liquid Aluminum. *Metals* **2022**, *12* (8), No. 1346.
(20) Levitas, V. I.; Pantoya, M. L.; Chauhan, G.; Rivero, I. Effect of the Alumina Shell on the Melting Temperature Depression for Aluminum Nanoparticles. *J. Phys. Chem. C* **2009**, *113* (32), 14088−14096.
(21) Mei, Q. S.; Wang, S. C.; Cong, H. T.; Jin, Z. H.; Lu, K. Pressure-Induced Superheating of Al Nanoparticles Encapsulated in Al2O3 Shells without Epitaxial Interface. *Acta Mater.* **2005**, *53* (4), 1059−1066.
(22) Rai, A.; Park, K.; Zhou, L.; Zachariah, M. R. Understanding the Mechanism of Aluminium Nanoparticle Oxidation. *Combust. Theory Modell.* **2006**, *10* (5), 843−859.
(23) Tohei, T.; Watanabe, Y.; Lee, H.-S.; Ikuhara, Y. First Principles Calculation of Thermal Expansion Coefficients of Pure and Cr Doped α-Alumina Crystals. *J. Appl. Phys.* **2016**, *120* (14), No. 142106.
(24) Balakrishnan, G.; Thirumurugesan, R.; Mohandas, E.; Sastikumar, D.; Kuppusami, P.; Song, J. I. Phase Transition and Thermal Expansion Studies of Alumina Thin Films Prepared by Reactive Pulsed Laser Deposition. *J. Nanosci. Nanotechnol.* **2014**, *14* (10), 7728−7733.
(25) Cabrera, N.; Mott, N. F. Theory of the oxidation of metals. *Rep. Prog. Phys.* **1949**, *12*, No. 163.
(26) Jackson, J. D. Classical Electrodynamics.
(27) Maier, J.; Wiley, J. Physical Chemistry of Ionic Materials: Ions and Electrons in Solids.
(28) Buchanan, R. C. *Ceramic Materials for Electronics*, 3rd ed.; CRC Press, 2004 DOI: 10.1201/9781315273242.
(29) García-Méndez, M.; Valles-Villarreal, N.; Hirata-Flores, G. A.; Farías, M. H. Study of Thermal Diffusion between Al2O3 and Al Thin Films. *Appl. Surf. Sci.* **1999**, *151* (1−2), 139−147.
(30) Campbell, T.; Kalia, R. K.; Nakano, A.; Vashishta, P.; Ogata, S.; Rodgers, S. Dynamics of Oxidation of Aluminum Nanoclusters Using Variable Charge Molecular-Dynamics Simulations on Parallel Computers. *Phys. Rev. Lett.* **1999**, *82* (24), 4866−4869.
(31) Christian, J. H.; Taylor, H. L. Ionic Diffusion at the Aluminum-Aluminum Oxide Interface. *J. Appl. Phys.* **1967**, *38* (10), 3843−3845.
(32) Paladino, A. E.; Kingery, W. D. Aluminum Ion Diffusion in Aluminum Oxide. *J. Chem. Phys.* **1962**, *37* (5), 957−962.
(33) Fielitz, P.; Ganschow, S.; Kelm, K.; Borchardt, G. Aluminium Self-Diffusion in High-Purity α-Al2O3: Comparison of Ti-Doped and Undoped Single Crystals. *Acta Mater.* **2020**, *195*, 416−424.
(34) Zalar, A.; Baretzky, B.; Dettenwanger, F.; Ruhle, M.; Panjan, P. Interdiffusion at the Al2O3/Ti Interface Studied in Thin-Film Structures. *Surf. Interface Anal.* **1998**, *26* (11), 861−867.
(35) Chowdhury, S.; Sullivan, K.; Piekiel, N.; Zhou, L.; Zachariah, M. R. Diffusive vs Explosive Reaction at the Nanoscale. *J. Phys. Chem. C* **2010**, *114* (20), 9191−9195.
(36) Park, K.; Lee, D.; Rai, A.; Mukherjee, D.; Zachariah, M. R. Size-Resolved Kinetic Measurements of Aluminum Nanoparticle Oxidation with Single Particle Mass Spectrometry. *J. Phys. Chem. B* **2005**, *109* (15), 7290−7299.

https://doi.org/10.1021/acs.jpcc.5c06533
J. Phys. Chem. C XXXX, XXX, XXX−XXX